Journal of Catalysis 414 (2022) 330–335

Contents lists available at ScienceDirect

Journal of Catalysis

journal homepage: www.elsevier.com/locate/jcat

Experimental probing of the effect of PFSA ionomer poisoning at different Pt loadings in a PEMFC

Fen Zhou [a,b], Hui Zhang [a,b], Shumeng Guan [a,b], Guangfu Li [a], Lei Xia [a,b], Mu Pan [a,b,*]

[a] Foshan Xianhu Laboratory of the Advanced Energy Science and Technology Guangdong Laboratory, Xianhu Hydrogen Valley, Foshan 528200, China
[b] State Key Laboratory of Advanced Technology for Materials Synthesis Processing, Wuhan University of Technology, Wuhan 430070, China

ARTICLE INFO

Article history:
Received 2 May 2022
Revised 15 September 2022
Accepted 19 September 2022
Available online 23 September 2022

Keywords:
Charge-transfer resistance (R_{ct})
Poisoning effect from Nafion
Pt loading
Sulfonate coverage
PEMFC

ABSTRACT

The charge-transfer resistance (R_{ct}) in electrochemical impedance spectroscopy (EIS) was applied as an activity indicator to study the suppression of rotating disk electrodes (RDEs) and membrane electrode assemblies (MEAs) with different Pt loadings by Nafion. The use of R_{ct} avoids the uncertainty in activity characterization caused by mass transfer in highly loaded catalyst agglomerates. Nafion exhibited a stronger poisoning effect at lower Pt loadings in both the RDEs and MEAs. The simultaneous reduction in working voltage further aggravates this poisoning, especially under low-Pt conditions. After poisoning, the normalized R_{ct} at 20 μg/cm^2 increased by 8 times at 0.9 V and 21 times at 0.82 V. When the Nafion adsorption coverage on the surface of Pt remained constant, the suppression of activity was enhanced as the Pt loading decreased. Therefore, it is critical to consider Nafion poisoning when constructing MEAs with low platinum loading and to take appropriate strategies to alleviate poisoning and achieve high-performance.

1. Introduction

One major impediment to the commercialization of fuel cells is the high cost of the precious metal Pt in the catalyst, which accounts for up to 40% of the total cost [1,2]. Therefore, the development of high-performance membrane electrode assemblies (MEAs) with low platinum is important for the commercialization of proton exchange membrane fuel cells (PEMFCs). However, reducing the Pt loading results in a significant decrease in performance [3–5]. This performance degradation is mainly caused by polarization induced by the PFSA ionomer thin film covering the Pt surface [6–9], Nafion for example, including poisoning by sulfonate on the side chain of Nafion [10].

The sulfonates on Nafion coordinate to Pt, occupying the active sites of oxygen reduction and reducing Pt utilization [11–20]. The activity suppression is related to the quantity of sulfonate adsorbed on the Pt surface, which is proportional to the coverage of the Nafion thin film on the Pt surface. Moreover, the activity of the catalyst decreases significantly with increasing Nafion content and finally reaches a plateau, where the residual activity is only half of the initial activity [7,19]. The poisoning effect is strongly dependent on the morphology of the catalyst [16,21]. Since Pt deposition inside the pores of porous carbon-supported Pt catalysts can be controlled and the Nafion coverage is limited, the poisoning effect is significantly lower than that of solid carbon-supported platinum catalysts [7]. Although the research on the suppression of Pt catalyst activity by Nafion is relatively sufficient, there have been no studies on the effect of Pt loading on Nafion poisoning, which is a necessary research topic in the development of high-performance MEAs with low Pt usage.

Current ex situ studies of Nafion poisoning are performed with a RDE. The area-specific activity (SA) and mass-specific activity (MA) calculated from the oxygen reduction kinetic current are general activity standards. When using these standards, according to Eq. (1), the tested apparent current must be corrected for mass transfer to determine the oxygen reduction kinetic current [22]. However, in studies of the effect of Pt loading on Nafion poisoning, RDEs with high Pt loading are thick enough that the mass transfer characteristics are no longer satisfied, introducing significant uncertainty into the tested activity[23–25]. Electrochemical impedance spectroscopy (EIS) is a sensitive method for distinguishing and analyzing charge and mass transfer processes, and it is often employed to study diffusion phenomena in fuel cell structures and catalyst kinetic behavior [26–29]. Springer et al. [30,31] presented a theoretical impedance spectroscopy study of the oxygen reduction reaction (ORR) on porous gas diffusion electrodes in a

* Corresponding author at: Foshan Xianhu Laboratory of the Advanced Energy Science and Technology Guangdong Laboratory, Xianhu Hydrogen Valley, Foshan 528200, China.
E-mail address: panmu@whut.edu.cn (M. Pan).

https://doi.org/10.1016/j.jcat.2022.09.019
0021-9517/

liquid agglomerated electrode model in 1989. Since then, EIS has been widely used to investigate fuel cell behaviors [29,31–36]. In addition to analyzing the diffusion properties of porous electrodes, the charge-transfer resistance (R_{ct}) in the EIS spectrum has been widely applied to analyze catalytic kinetic issues or as an indicator of catalyst activity [37–41]. Kim and Zhang et al. [26,42] used the R_{ct} in EIS as a metric to evaluate the oxygen reduction activity of non-platinum catalysts. In recent years, our research group proposed R_{ct} in EIS as an indicator for evaluating the electrochemical activity of ORR catalysts in PEMFCs at the rated voltage [37,38]. The effectiveness of the R_{ct} indicator has been studied using Pt/C and PtCo/C catalysts.

$$j_k = \frac{j_d \times j}{j_d - j} \quad (1)$$

where j is the apparent current, j_d is the limit current, and j_k is the kinetic current.

There is no need for data correction since the charge transfer impedance can be directly obtained using the EIS test as an indicator of catalyst activity. In our work, R_{ct} is used as the activity indicator, and ex situ RDE and in situ MEA tests are performed to explore Nafion poisoning under different Pt loadings. The sulfonate adsorption coverage on the Pt surface is investigated to establish the correlation between the Nafion poisoning effect and the sulfonate coverage under different Pt loadings.

2. Experimental

Preparation of RDEs. Five milligrams of Pt/V catalyst (30% Pt/V from TKK) was ultrasonically dispersed in an ice water bath for 20 min in a mixture consisting of Nafion solution (5 wt%, DuPont), deionized water (>15 M·cm), and isopropanol (99.9 wt%, Sinopharm Group Chemistry Co., ltd.). An appropriate amount of dispersed ink was dropped on a clean glassy carbon electrode with a diameter of 5 mm to prepare working electrodes. Therein, Pt loadings of 20 μg/cm^2, 30 μg/cm^2 and 40 μg/cm^2 were investigated to identify the roles of Nafion ionomer in the RDE system. The weight ratio of ionomer to carbon support (I/C) was 0.8; this value is generally used by most researchers [18,43]. The electrodes were spin-dried in air at 400 rpm and then dried at ambient temperature for 24 h. The specific preparation of the electrodes with Nafion and without Nafion was performed according to previous work [44]. The electrodes were labeled Pt/V-w-*x* (*x* represents the Pt loading). For comparison, an additional set of electrodes without Nafion was prepared and labeled Pt/V-w/o-*x*.

Preparation of MEAs. Using the same catalyst as that used for the RDEs, catalyst layers with Pt loadings of 0.05 ± 0.008 mg/cm^2, 0.1 ± 0.008 mg/cm^2, and 0.13 ± 0.007 mg/cm^2 were created and served as the cathode in a PEMFC. The preparation method was described in earlier works [41]. The Pt loading (60% Pt/C, TKK) in the anode was 0.4 mg/cm^2. The I/C of both the cathode and anode catalyst layers was 0.8, the same as in the RDE. The prepared cathode and anode catalyst layers and proton exchange membrane (PEM) were used to prepare a catalyst-coated membrane (CCM) via the hot pressing decal transfer method. The CCM was prepared with a gas diffusion layer (GDL) to form an MEA. Each MEA had an active area of 25 cm^2. The catalyst inks used to obtain cathodes with different Pt loadings were the same, and the Pt loading was controlled by changing the thickness of the catalyst layer.

Electrochemical characterizations. All RDE tests were performed on an electrochemical workstation (CHI660e, Shanghai Chenhua Instrument Co., Ltd.). The electrolyte was 0.1 M perchloric acid solution ($HClO_4$). A platinum black electrode and a homemade reversible hydrogen electrode were employed as the counter electrode and the reference electrode, respectively. To achieve relatively steady performance, the prepared working electrode was activated in N_2-saturated 0.1 M $HClO_4$ using cyclic voltammetry (CV) at a scanning rate of 0.1 V/s in a potential range of 0 V to 1.2 V. CV measurements were then performed at 0.05 V/s to evaluate the ionomer-dependent electrochemical active surface area (ECSA) of Pt/C. Finally, the EIS test was carried out under different voltages with 10% AC amplitude and frequencies ranging from 10000 Hz to 0.1 Hz at 1600 rpm under O_2-saturated conditions.

Fuel cell operation. All single-cell tests were conducted on an automated Greenlight Innovation fuel cell test station (G20, Canada). Prior to the operation, the fuel cells were conditioned at rated power for 8 h under 80 °C, 75% relative humidity (RH), and a back pressure of 250 kPa_{abs}, with hydrogen and air fed into the anode and cathode, respectively[45]. The CV data were recorded at 30 ℃ and 100% RH. The fuel cell was purged with H_2 and N_2 at a flow rate of 200 sccm. The hydrogen crossover currents were obtained from linear scanning voltammetry (LSV) curves, which were obtained under the same conditions as CV, but at 80 °C. The EIS tests were performed on a Gamry Ref.5000 potentiostat using current control mode with an amplitude of 10% and a frequency range of 20000 ~ 0.5 Hz. The test conditions were 80 °C, 100% RH, 250 kPa_{abs}, and H_2/O_2 flow rates of 1500/2500 sccm. The large gas flow with high backpressure was employed to minimize the effect of the catalyst layer thickness on mass diffusion.

The method used to test the adsorption coverage of sulfonate on the Pt surface by replacing sulfonates with CO was described in earlier research works [8,46]. Since in $HClO_4$, the anion ClO_4^- can also adsorb onto the Pt surface, which would interfere with the test results, the measurements were not performed with the RDEs [46].

3. Results and discussion

To screen the Nafion ionomer effect on ECSA and the intrinsic catalytic activity, dispersed catalyst ink with/without Nafion as an additive was dropwise deposited on a clean glass-carbon RDE, and electrochemical measurements were carried out in 0.1 M $HClO_4$. The typical cyclic voltammograms in Fig. 1(a, b) exhibit the strong dependence of the recorded current on the applied catalyst loading. Based on the hydrogen adsorption/desorption behavior of the Pt-based catalyst, the ECSA was calculated and is shown in Fig. 1(c, d)[47]. For the samples without Nafion, the ECSA slightly decreased with increasing Pt loading. Apparently, high loading increases the thickness of the catalyst layer, increasing the interfacial resistance for electron and proton transport.

The average ECSA values of Pt/V-w/o and Pt/V-w electrodes with various Pt loadings were 80.61 m^2/g_{Pt} and 78.56 m^2/g_{Pt}, respectively. Note that the supplementation of protons is not as sufficient or convenient from Nafion in aqueous $HClO_4$ electrolyte, although Nafion is widely used as a solid polymer electrolyte for proton conductivity in PEMFCs. In contrast, Pt particles without Nafion are in direct contact with the $HClO_4$ solution, which indicates high accessibility to protons. The same effect of Nafion on ECSA was also verified in other research work [7].

R_{ct}, as an essential descriptor for ORR activity, was extracted by fitting the EIS results (Fig. S1, Supporting Information). Fig. 2 (a) clearly shows that the R_{ct} of the Pt/V-w electrode increased with decreasing Pt loading. In principle, R_{ct} is inversely proportional to the accessible active area of the Pt electrode [37]. For the same catalysts, R_{ct} normalized by ECSA will theoretically remain unchanged without varying measurement conditions, as observed from the Pt/V-w/o samples, especially at low potentials (Fig. 2(b)). Moreover, only a slight change in the normalized R_{ct} occurred at high potentials. R_{ct} exhibited the trend Pt/V-w/o-20 > Pt/V-w/o-30 > Pt/V-w/o-40. The increased

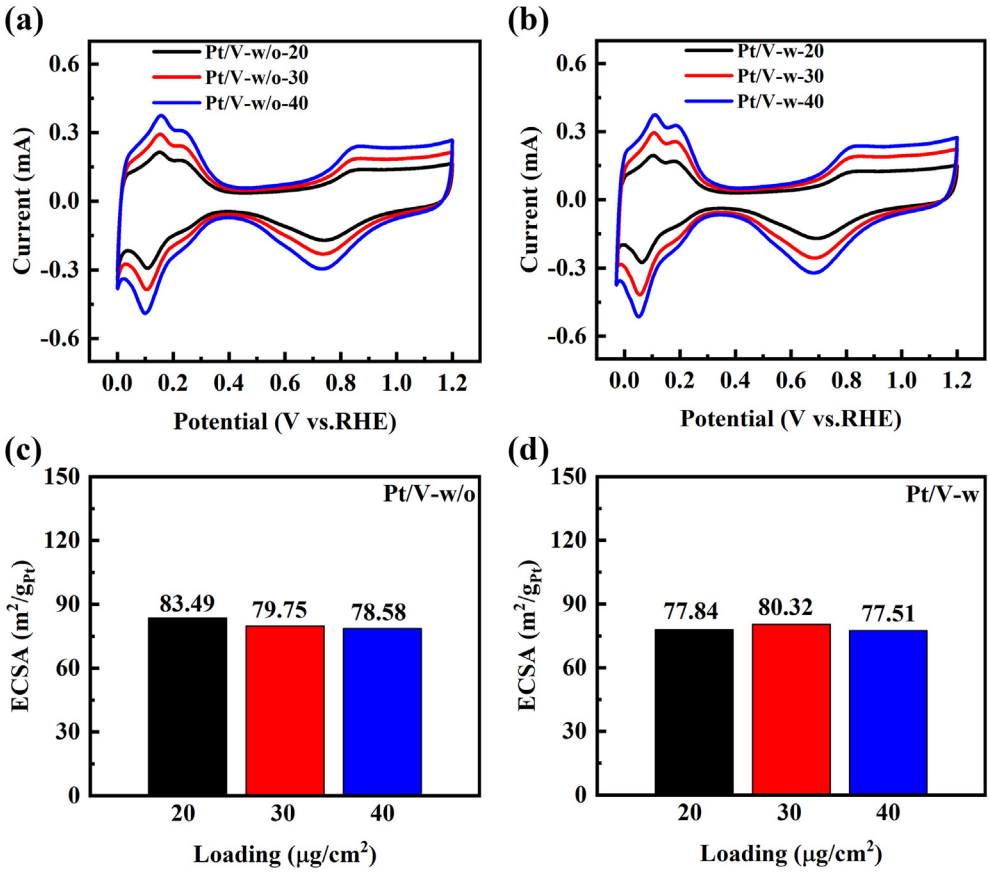

Fig. 1. Cyclic voltammograms of (a) Pt/V-w/o electrodes and (b) Pt/V-w electrodes; ECSA histogram of (c) Pt/V-w/o electrodes and Pt/V-w electrodes as a function a function of Pt loading.

normalized R_{ct} with the reduction in Pt loading might be attributed to the changed ORR proceeding pathway and products selectivity [48,49].

When Nafion was used in the RDE, the R_{ct} results without/with ECSA normalization both increased significantly with decreasing Pt loading (Fig. 2(c, d)). Obviously, the Nafion-containing electrode at lower Pt loading suffered from more severe polarization loss. The results of the Pt loading-versus-activity study are clearly different from the conclusions of earlier work that specific activity and mass activity served as activity indicators [50]. In particular, our observation shows the significance of the Nafion effect on R_{ct} rather than ECSA, suggesting the high validity of R_{ct} as an indicator of catalyst utilization.

To more clearly illustrate the effect of Nafion poisoning, the normalized R_{ct} ratio curves of Pt/V-w and Pt/V-w/o electrodes with the same loading are plotted in Fig. 3(a). As the applied potential decreased, the slope of the ratio became steeper, corresponding to an increased poisoning effect. The ratio of Pt/V-40 increased from 6 at 0.9 V to 9 at 0.82 V, while that of Pt/V-20 increased from 8 at 0.9 V to 21 at 0.82 V, indicating that the Nafion additive has an outsized poisoning effect at low Pt loadings. This result may be due to the higher output current density at a lower rated operating voltage, requiring more active sites [9]. There are insufficient Pt active sites when using a low Pt loading. The change in normalized R_{ct} between Pt/V-w/o-40 and Pt/V-w/o-20 seems nearly independent of the applied potential, and the magnification is approximately 1.3 in Fig. 3(b). The electrodes with Nafion exhibited a considerable change, especially at low potentials. For instance, the normalized R_{ct} of Pt/V-w-20 at 0.82 V was approximately 3.34 times larger than that of Pt/V-w-40.

To explore whether the observed R_{ct} trend can be attributed to the state of sulfonate adsorption coverage, the R_{ct} and sulfonate adsorption rates were tested in MEAs. Fig. S2a shows the CV curves and corresponding ECSA of the MEAs in a PEMFC. For ease of comparison, all CV curves were corrected for background current [51]. The MEA measurements reveal that Pt loading had no important impact on ECSA, consistent with the RDE observations. In contrast, R_{ct} exhibited a strong dependence on Pt loading, as shown in Fig. 4. The Tafel plots in Fig. S3d were obtained under pure oxygen supply and with correction for the high-frequency resistance (HFR), electrode proton resistance, and hydrogen crossover. As the Pt loading decreased from 0.13 mg/cm^2 to 0.05 mg/cm^2, the Tafel slope increased from 70.7 mV/dec to 78.89 mV/dec. The increase in Tafel slope also demonstrates the delay in reaction kinetics.

The sulfonate adsorption coverage in MEAs with various Pt loadings (Fig. 5) was determined to study the interfacial properties on the Pt-Nafion surface. For all studied MEAs, the same catalyst slurry was applied in the preparation of the catalyst layers. By using the same coating method, three different catalyst layers were fabricated with different coating thicknesses. After the coating step was completed, the catalyst layer was quickly dried and shaped so that the distribution state of the catalyst and Nafion could be considered [52]. Fig. 5(a) and Fig. 5(b) show the current curves of CO displacement and CO stripping, respectively. For comparison, the background current has been subtracted from the curves in Fig. 5 (a) [46]. With the decrease in Pt loading, the charge generated by displaced sulfonate on the Pt surface decreases, and the charge generated by CO oxidative stripping also declines. After the changes in electric charge were normalized by the Pt loading, as shown in Fig. 5(c), the normalized electric charges of displacement

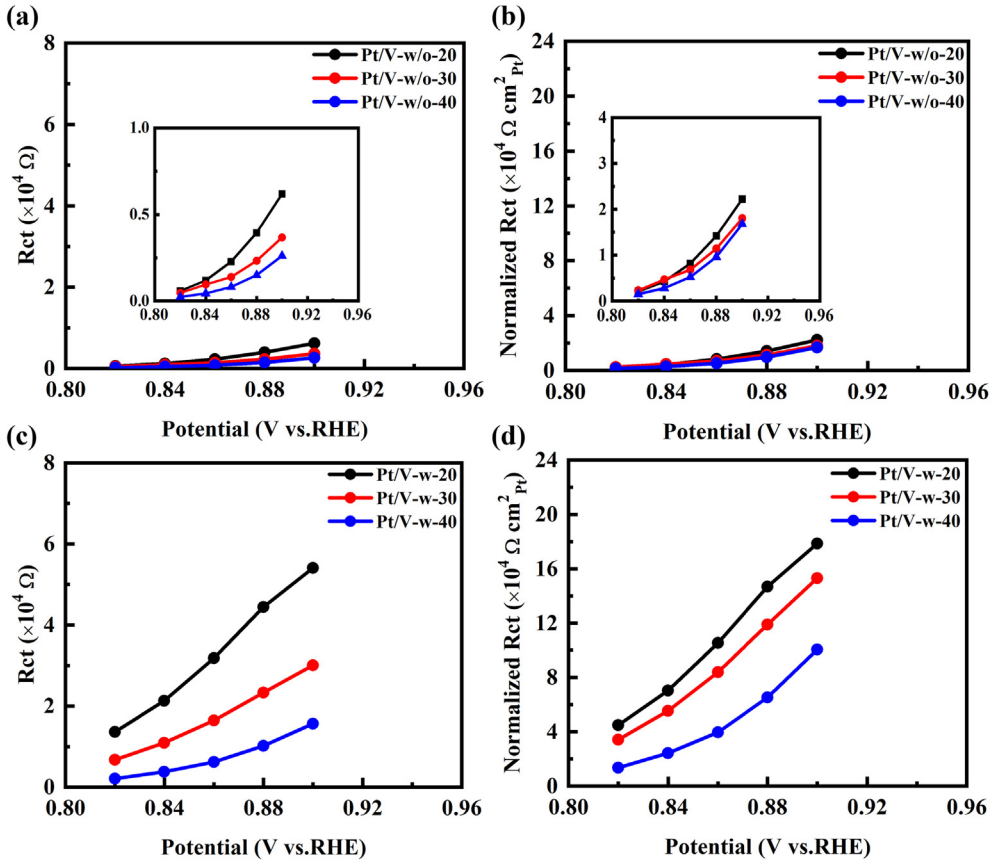

Fig. 2. R_{ct} versus potential at different Pt loadings (a) Pt/V-w/o electrodes; (b) Pt/V-w/o electrodes and curves of normalized R_{ct} versus potential at different Pt loadings (c) Pt/V-w electrodes; (d) Pt/V-w electrodes.

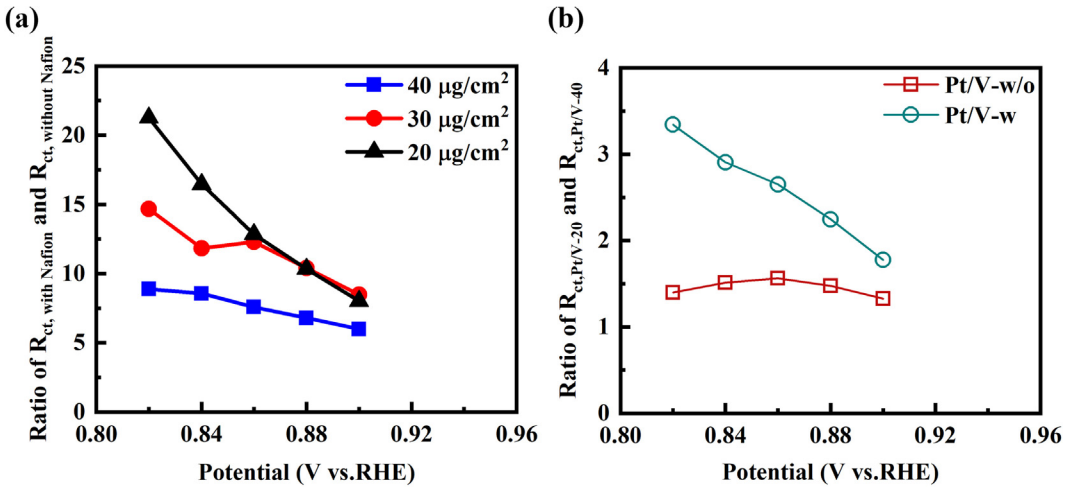

Fig. 3. Ratio curves of (a) normalized $R_{ct,withNafion}$ and $R_{ct,withoutNafion}$ for electrodes with different Pt loadings and (b) $R_{ct,Pt/V-20}$ and $R_{ct,Pt/V-40}$ for electrodes with Nafion and without Nafion.

and oxidative stripping remained nearly constant. As presented in Fig. 5(d), the calculated adsorption coverage of sulfonate on the Pt surface was 12.04%, 12.24% and 12.44% for 0.05, 0.1 and 0.13 mg/cm^2 Pt loadings, respectively. It can be concluded that changes in Pt loading do not influence the sulfonate adsorption rate on the Pt surface.

It was reported that sulfonates on the Nafion side chain are prone to adsorption on the Pt surface, where they occupy active sites and hinder the dissociation of oxygen molecules [10]. Under the same Pt loading conditions, the electrode with Nafion is more likely to generate hydrogen peroxide than the electrode without Nafion [12,13]. Zhang et al. demonstrated that the Pt coordination environment could control ORR products selectivity [53]. Moreover, the coordination of sulfonate with Pt would not only poison the Pt atoms at the adsorption site, but also poison the adjacent Pt atoms [9]. As a result, a small change in the amount of sulfonate coverage will lead to a large decrease in activity [16,18]. Nafion reduces the active sites and sacrifices the utilization of Pt, which

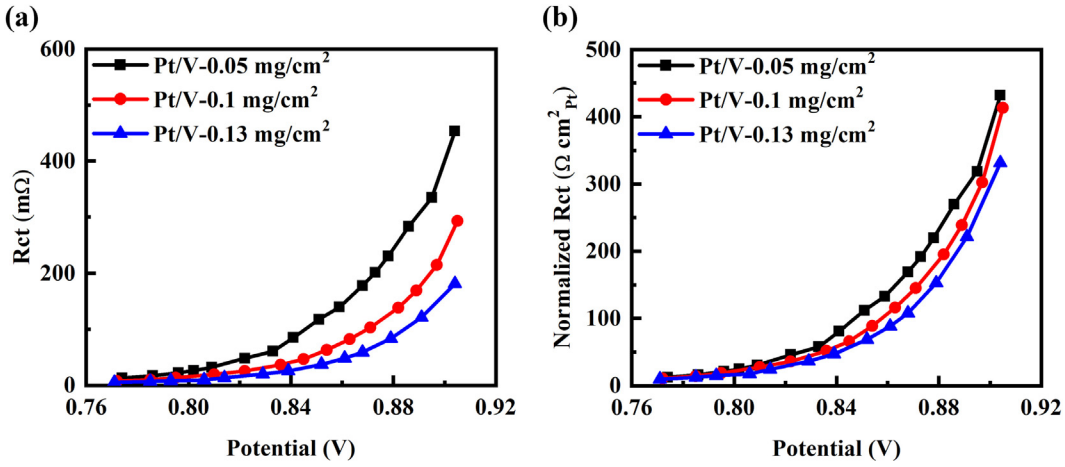

Fig. 4. MEAs with different Pt loadings: (a) curves of R_{ct} versus potential; (b) curves of normalized R_{ct} versus potential.

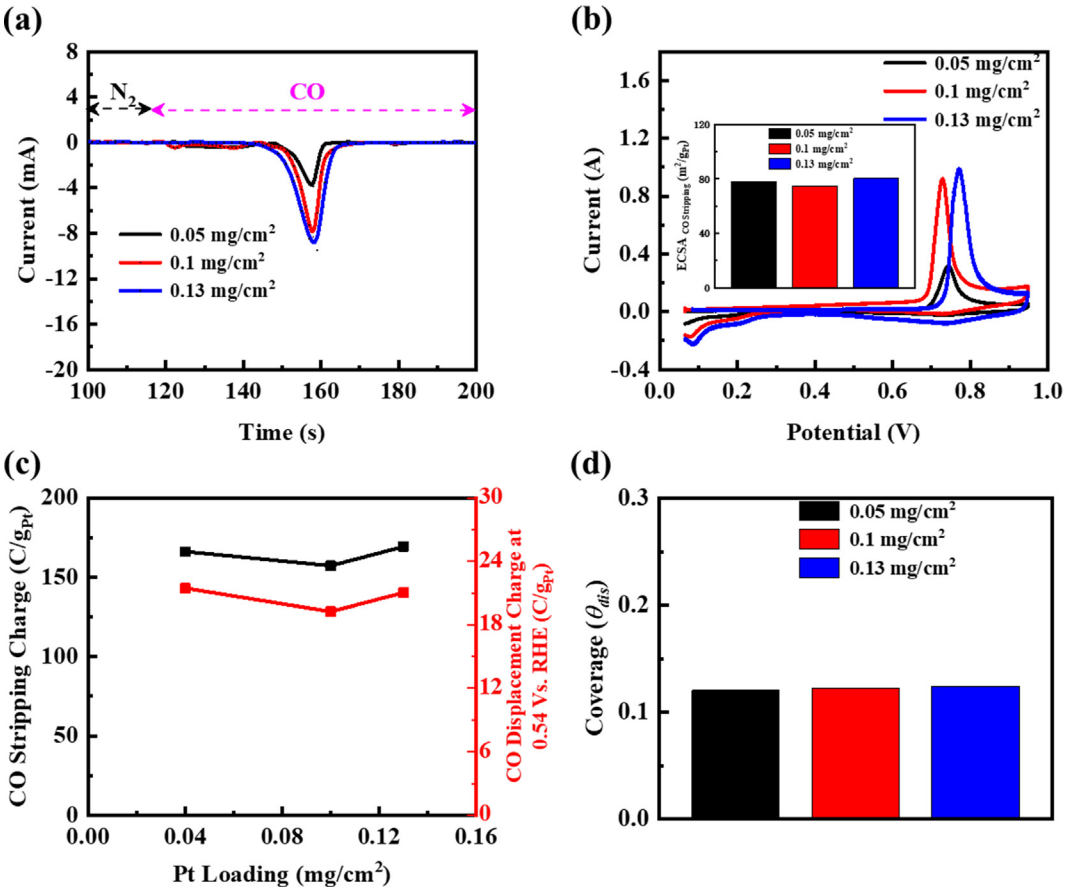

Fig. 5. MEAs with different Pt loadings: (a) CO displacement current and time curves; (b) CO stripping cyclic voltammograms; (c) CO displacement charge per unit mass of Pt (right axis) and CO stripping charge (left axis); (D) sulfonate adsorption coverage on the Pt surface.

is equivalent to reducing the loading of Pt. Therefore, the loading effect should also apply in electrodes without Nafion, which can be obviously observed from Fig. 2. The normalized R_{ct} for electrodes without Nafion still exhibited the same trends as electrodes with Nafion. Many researches have investigated the Pt loading effect on ORR [48,49,54,55]. The general view is that as the Pt loading decreases, the ORR will be promoted to proceed via two-electron pathway, leading to a higher yield of hydrogen peroxide. The hydrogen peroxide is considered to be always produced during the ORR on Pt [56]. When the active sites continue to decrease, the generated hydrogen peroxide cannot be reduced in time, resulting in the accumulation of hydrogen peroxide [48], and the ORR path changes accordingly. It was reported that the electrochemical mechanisms related to the reaction of hydrogen peroxide during the ORR could limit the PEFC performance [57]. Therefore, we believe that when the Pt loading or effective active area decreases, the increase of normalized R_{ct} could be ascribed to the change of ORR proceeding way. However, the detailed ORR mechanism

changes are not well understood yet and deserve further exploration.

Although the adsorption rate of sulfonate is only 12%, any factor that reduces the effective Pt active area is fatal for MEAs with low Pt loading [58]. Based on the results presented in Fig. 4 and Fig. 5, although the sulfonate coverage of the electrodes remained unchanged, the R_{ct} of the electrode with lower Pt loading suffered from more serious poisoning. Therefore, poisoning by sulfonate on the side chain of Nafion should be considered when constructing MEAs with low Pt loading and high performance. More importantly, appropriate strategies should be taken to alleviate this poisoning without affecting the transport of protons and oxygen [16], which greatly favors the selection of MEAs with low Pt loading to achieve high performance.

4. Conclusion

The Pt loading effect on Nafion-induced activity suppression in RDEs and MEAs was investigated via our developed EIS technique. The use of R_{ct} in the EIS spectrum could avoid uncertainty in activity characterization, which cannot avoid mass transport loss, especially in highly loaded catalyst agglomerates. Our observations reveal that a reduction in Pt loading amplifies poisoning by Nafion. After Nafion was added to the electrode, the normalized R_{ct} for a Pt loading of 40 $\mu g/cm^2$ increased by 6 times, while that for a Pt loading of 20 $\mu g/cm^2$ increased by 8 times at the same potential. Moreover, a lower operating voltage induces more severe poisoning. The normalized R_{ct} of the electrode with Nafion at a Pt loading of 20 $\mu g/cm^2$ was 6 times higher at 0.9 V than that without Nafion, and this ratio even increased to 21 times at 0.82 V. Even under the premise that the adsorption coverage of sulfonate on the catalyst surface remains unchanged, the poisoning effect of Nafion increases with decreasing Pt loading.

Data availability

No data was used for the research described in the article.

Declaration of Competing Interest

The authors declare that they have no known competing financial interests or personal relationships that could have appeared to influence the work reported in this paper.

Acknowledgements

This work was financially supported by Guangdong Provincial Key Field R&D Programme (grant numbers 2021B0707040001).

Appendix A. Supplementary data

Supplementary data to this article can be found online at https://doi.org/10.1016/j.jcat.2022.09.019.

References

[1] D. Papageorgopoulos, in the DOE Hydrogen and Fuel Cells Program 2018 Annual Merit Review and Peer Evaluation Meeting, Washington, D.C (2018).
[2] Y. Wang, D.F.R. Diaz, K.S. Chen, Z. Wang, X.C. Adroher, Mater. Today 32 (2020) 178–203.
[3] J.P. Owejan, J.E. Owejan, W. Gu, J. Electrochem. Soc. 160 (2013), F824–F833.
[4] A. Kongkanand, M.F. Mathias, J. Phys. Chem. Lett. 7 (2016) 1127–1137.
[5] X. Deng, C. Huang, X.D. Pei, B. Hu, W. Zhou, Int. J. Hydrogen Energy 47 (2022) 1529–1542.
[6] S.S. Kocha, J.W. Zack, S.M. Alia, K. Neyerlin, B.S. Pivovar, ECS Trans. 50 (2013) 1475–1485.
[7] K. Shinozaki, M. Yu, B.S. Pivovar, S.S. Kocha, J. Power Sources 325 (2016) 745–751.
[8] A. Perego, A. Avid, D.N. Mamania, Y. Chen, P. Atanassov, H. Yildirim, M. Odgaard, I.V. Zenyuk, Appl. Catal. B Environ. 301 (2022) 120810.
[9] S. Jomori, K. Komatsubara, N. Nonoyama, M. Kato, T. Yoshida, J. Electrochem. Soc. 160 (2013), F1067–F1073.
[10] K. Kodama, K. Motobayashi, A. Shinohara, N. Hasegawa, K. Kudo, R. Jinnouchi, M. Osawa, Y. Morimoto, ACS Catal. 8 (2018) 694–700.
[11] A. Kabasawa, H. Uchida, M. Watanabe, Electrochem. Solid State Lett. 11 (2008), B190–B192.
[12] H. Yano, E. Higuchi, H. Uchida, M. Watanabe, J. Phys. Chem. B 110 (2006) 16544–16549.
[13] A. Ohma, K. Fushinobu, K. Okazaki, Electrochim. Acta 55 (2010) 8829–8838.
[14] R. Subbaraman, D. Strmcnik, A.P. Paulikas, V.R. Stamenkovic, N.M. Markovic, Chemphyschem 11 (2010) 2825–2833.
[15] A. Chowdhury, A. Bird, J. Liu, I.V. Zenyuk, A. Kusoglu, C.J. Radke, A.Z. Weber, A. C.S. Appl, Mater. Inter. 13 (2021) 42579–42589.
[16] H. Yamada, H. Kato, K. Kodama, J. Electrochem. Soc. 167 (2020) 084508.
[17] J.A. Keith, T. Jacob, Angew. Chem. Int. Ed. 49 (2010) 9521–9525.
[18] T. Takeshita, Y. Kamitaka, K. Shinozaki, K. Kodama, Y. Morimoto, J. Electroanal. Chem. 871 (2020) 114250.
[19] C. Liu, T. Uchiyama, N. Nagata, M. Arao, K. Yamamoto, T. Watanabe, X. Gao, H. Imai, S. Katayama, S. Sugawara, K. Shinohara, K. Oshima, S. Sakurai, Y. Uchimoto, A.C.S. Appl, Energ. Mater. 4 (2021) 1143–1149.
[20] Y. Kamitaka, T. Takeshita, Y. Morimoto, Catalysts 8 (2018) 230.
[21] V. Yarlagadda, M.K. Carpenter, T.E. Moylan, R.S. Kukreja, R. Koestner, W. Gu, L. Thompson, A. Kongkanand, ACS Energy Lett. 3 (2018) 618–621.
[22] H.A. Gasteiger, S.S. Kocha, B. Sompalli, F.T. Wagner, Appl. Catal. B Environ. 56 (2005) 9–35.
[23] T.J. Schmidt, H.A. Gasteiger, in: Handbook of Fuel Cells - Fundamentals, Technology and Applications, Wiley, 2003, p. 316.
[24] J. Perez, E. Gonzalez, E. Ticianelli, Electrochim. Acta 44 (1998) 1329–1339.
[25] F. Gloaguen, P. Convert, S. Gamburzev, O. Velev, S. Srinivasan, Electrochim. Acta 43 (1998) 3767–3772.
[26] Y.E. Song, S. Lee, M. Kim, J. Na, J. Lee, J. Lee, J.R. Kim, J. Power Sources 451 (2020) 227816.
[27] Y. Qiu, Z. Hu, H. Li, Q. Ren, Y. Chen, S. Hu, Chem. Eng. J. 430 (2022) 132769.
[28] J. Liu, Z. Gong, C. Allen, W. Ge, H. Gong, J. Liao, J. Liu, K. Huang, M. Yan, R. Liu, Chem. Catal. 1 (2021) 1291–1307.
[29] A.A. Kulikovsky, M. Eikerling, J. Electroanal. Chem. 691 (2013) 13–17.
[30] T.E. Springer, I.D. Raistrick, J. Electrochem. Soc. 136 (1989) 1594–1603.
[31] T.E. Springer, T.A. Zawodzinski, M.S. Wilson, S. Gottesfeld, J. Electrochem. Soc. 143 (1996) 587–599.
[32] M. Eikerling, A.A. Kornyshev, J. Electroanal. Chem. 453 (1998) 89–106.
[33] M. Eikerling, A.A. Kornyshev, J. Electroanal. Chem. 475 (1999) 107–123.
[34] M. Ciureanu, R. Roberge, J. Phys. Chem. B 105 (2001) 3531–3539.
[35] S.J. Lee, S. Mukerjee, J. McBreen, Y.W. Rho, Y.T. Kho, T.H. Lee, Electrochim. Acta 43 (1998) 3693–3701.
[36] F. Capitanio, S. Siracusano, A. Stassi, V. Baglio, A.S. Arico, A.C. Tavares, Int. J. Hydrogen Energy 39 (2014) 8026–8033.
[37] Y. Rao, C. Cai, J. Tan, M. Pan, J. Electrochem. Soc. 166 (2019) F351–F356.
[38] L. Xia, F. Zhou, H. Zhang, Z. Liu, G. Li, S. Li, M. Pan, J. Electrochem. Soc. 169 (2022) 054533.
[39] L. Sahoo, S. Mondal, A. Gloskovskii, A. Chutia, U.K. Gautam, J. Mater. Chem. A 9 (2021) 10966–10978.
[40] S. Liu, S. Li, R. Wang, Y. Rao, Q. Zhong, K. Hong, M. Pan, J. Electrochem. Soc. 166 (2019), F1308–F1313.
[41] S. Guan, F. Zhou, S. Du, M. Pan, J. Electrochem. Soc. 169 (2022) 014504.
[42] J. Zhang, L. Zhang, C.W.B. Bezerra, H. Li, Z. Xia, J. Zhang, A.L.B. Marques, E.P. Marques, Electrochim. Acta 54 (2009) 1737–1743.
[43] A. Kobayashi, T. Fujii, C. Harada, E. Yasumoto, K. Takeda, K. Kakinuma, M. Uchida, A.C.S. Appl, Energ. Mater. 4 (2021) 2307–2317.
[44] K. Shinozaki, J.W. Zack, S. Pylypenko, B.S. Pivovar, S.S. Kocha, J. Electrochem. Soc. 162 (2015), F1384–F1396.
[45] A. Orfanidi, P. Madkikar, H.A. El-Sayed, G.S. Harzer, T. Kratky, H.A. Gasteiger, J. Electrochem. Soc. 164 (2017), F418–F426.
[46] T.R. Garrick, T.E. Moylan, V. Yarlagadda, A. Kongkanand, J. Electrochem. Soc. 164 (2017), F60–F64.
[47] Y. Chen, Q. Zhong, G. Li, T. Tian, J. Tan, M. Pan, Ionics 24 (2018) 3905–3914.
[48] K. Ke, T. Hatanaka, Y. Morimoto, Electrochim. Acta 56 (2011) 2098–2104.
[49] Y. Zhang, J. Li, Q. Peng, P. Yang, Q. Fu, X. Zhu, Q. Liao, Electrochim. Acta 429 (2022) 140953.
[50] Y. Rao, F. Zhou, K. Fu, W. Guo, M. Pan, Int. J. Electrochem. Sci. 12 (2017) 4630–4639.
[51] M.D. Edmundson and F. C. Busby, in *11th Polymer Electrolyte Fuel Cell Symposium (PEFC) Under the Auspices of the 220th Meeting of the ECS*, p. 661-671, Boston, MA (2011).
[52] Y. Liu, C. Ji, W. Gu, D.R. Baker, J. Jorne, H.A. Gasteiger, J. Electrochem. Soc. 157 (2010), B1154–B1162.
[53] J. Zhao, C. Fu, K. Ye, Z. Liang, F. Jiang, S. Shen, X. Zhao, L. Ma, Z. Shadike, X. Wang, J. Zhang, K. Jiang, Nat. Commun. 13 (2022) 685.
[54] M. Inaba, H. Yamada, J. Tokunaga, A. Tasaka, Electrochem. Solid-State Lett. 7 (2004), A474–A476.
[55] A. Bonakdarpour, T.R. Dahn, R. Atanasoski, M.K. Debe, J.R. Dahn, Electrochem. Solid-State Lett. 11 (2008) B208.
[56] A. Gomez-Marin, J. Feliu, T. Edson, ACS Catal 8 (2018) 7931–7943.
[57] S. Cruz-Manzo, R. Chen, P. Greenwood, J. Electroanal. Chem. 745 (2015) 28–36.
[58] A.Z. Weber, A. Kusoglu, J. Mater. Chem. A 2 (2014) 17207–17211.